MICROSCALE TRANSPORT PHYSICS DURING ATOMIC FORCE MICROSCOPY MASS SPECTROMETRY AND IMPROVED SAMPLING EFFICIENCY

Hyunkyu Moon[1], Troy J. Comi[2], Sage J. B. Dunham[2], Beomjin Kwon[1], Jonathan V. Sweedler[2], and William P. King[1]

[1]Department of Mechanical Science and Engineering, University of Illinois at Urbana-Champaign, Urbana, IL, USA

[2]Department of Chemistry, University of Illinois at Urbana-Champaign, Urbana, IL, USA

ABSTRACT

This paper reports improvements of atomic force microscopy (AFM) mass spectrometry (MS), in which ~1 attoliter of analyte is desorbed by a heated AFM cantilever tip and analyzed with a mass spectrometer. Decoupling the AFM sampling apparatus from the MS system enabled analysis of the microscale transport physics independent of analyte ionization efficiency. Using this approach, we find that the transport efficiency is governed by the air velocity during sampling, and not mass flow rate as reported in the literature. We also find that an unheated sampling tube results in higher efficiency compared to a heated tube. Optimization of the transport parameters improved the system efficiency by 2.5-fold over the state of the art.

KEYWORDS

Atomic force microscopy, mass spectrometry, heated cantilever, thermal desorption, transport physics

INTRODUCTION

Mass spectrometry offers unparalleled chemical information from complex samples and is well suited to characterizing small-volume chemically complex samples such as individual cells [1-2]. However, sampling intact biological molecules from submicron-sized areas while efficiently introducing the sample to the mass spectrometer remains a challenge. AFM-MS overcomes this problem by combining the exceptional spatial resolution of AFM with the advantages of MS [3-6]. In AFM-MS, an AFM cantilever tip scans a surface and applies local heating to desorb a molecular sample, which is captured and analyzed by MS [3-5]. Typically, the sample is drawn through a tube and directly ionized before introduction into the mass analyzer [3-5]. Researchers have explored several different ionization techniques for AFM-MS. For example, Ovchinnikova et al. employed electrospray ionization and successfully analyzed caffeine with 250 nm spatial resolution [4]. Atmospheric pressure chemical ionization was also employed for analyzing ink and polymer blends with 2.5 μm spatial resolution [4-5]. At present, the transport physics of the sampling process are not well understood, preventing optimization of figures of merit necessary for fundamental improvements to AFM-MS.

In this work, we report the transport physics in an AFM-MS system, which efficiently collects the thermally desorbed sample using a tube. Transport efficiency was measured at different experimental parameters to find an optimal condition for AFM-MS. Decoupling the sampling process from MS analysis allows independent optimization of molecular sampling and mass analysis to provide overall improved performance. We achieved transport efficiency of 3.5% with the optimized experimental parameters, which represents a 2.5-fold improvement in efficiency over the current state of the art [3, 9].

SYSTEM AND MEASUREMENTS

Figure 1 illustrates the experimental setup. The sample is thermally desorbed by the heated AFM cantilever tip, transferred through a 21 cm-long stainless steel tube, and collected on a microwell plate in a vacuum chamber. A pressure difference is maintained between the tube inlet and outlet to drive the airflow through the tube. A sample of 9-aminoacridine (9AA; SigmaAldrich) was used in the optimization experiments described here. 9AA is a commonly used matrix for matrix-assisted laser desorption/ionization (MALDI) and is also fluorescent. The system was operated at room temperature, except during experiments to assess the influence of heating the transfer tubing. For the tube heating experiments, the stainless steel tube was heated by a nichrome wire wrapped around the tube regulated with a temperature controller. The AFM cantilever temperature was calibrated using Raman spectroscopy before the thermal desorption operation [7]. The heated AFM cantilever tip scanned over the sample at a cantilever temperature of 600 ˚C with scan length 80 μm. The desorbed 9AA was collected on a 96-well plate for subsequent MS or fluorescence analysis.

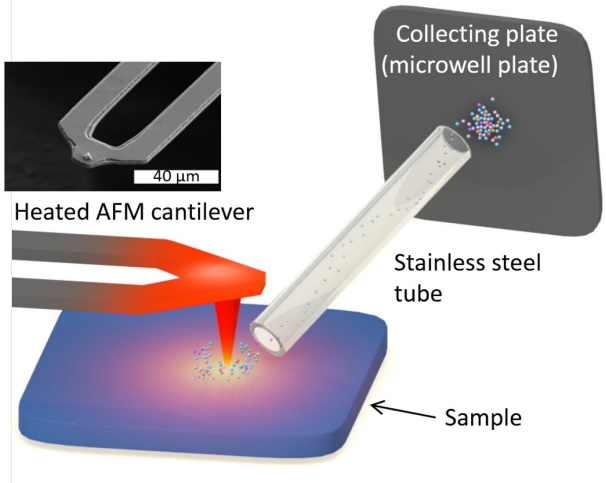

Figure 1: Schematic of the experimental setup. Local heating from an AFM tip results in desorption of a microscale sample volume, which is drawn through a stainless steel tube and collected on the sample collecting plate. The tip and sample are at atmospheric pressure, and the chamber containing the plate is maintained at a lower pressure to control the flow rate through the tube.

Air flow into the chamber was measured with a gas mass flow meter connected in series between the stainless steel tube and the vacuum chamber. A pressure gauge measured the pressure inside the chamber during operation. The air flow rate was controlled by adjusting pump inlet valve. The chamber pressure was calibrated as a function of air flow rate.

Samples were prepared from a solution of 2 mg/mL 9AA in ethanol. 1 µL of 9AA solution was dropped on a silicon substrate and dried at room temperature overnight, which solidified with an average thickness of ~ 20 µm.

The system transport efficiency, defined as the ratio of collected mass to desorbed mass, was measured using a three-dimensional optical microscope and a fluorescence microplate reader. The desorbed mass was calculated by evaluating three-dimensional optical microscopy measurements of the sample before and after desorption as shown in Figure 2. The collected mass was determined with a fluorescence microplate reader using an excitation wavelength of 400 nm and an emission wavelength of 470 nm. The selected wavelengths were chosen to maximize the signal-to-noise ratio of a standard 9AA solution. Figure 3 shows the calibration curve for the florescence intensity as 9AA concentration varies from 0 – 10 ng/mL. The fluorescence signal linearly increases with the 9AA concentration in the range of interest. 9AA collected in the microwell plate was dissolved in 100 µL ethanol, then its mass was determined from the fluorescence intensity of the solution and the calibration curve. The ethanol solvent without 9AA also shows weak fluorescence signal which dictates the noise floor.

EXPERIMENTAL RESULTS

Figure 4(a) shows the transport efficiency measured at different flow rates from 400 mL/min to 10000 mL/min, when the distance between the tube inlet and the sample was 3.5 mm. The transport efficiency initially increases with increasing flow rate, and starts to decrease when the air flow rate is larger than 3500 mL/min. This flow rate corresponds with a Reynolds number of 2300 for a tube with an inner diameter (ID) of 2.1 mm, which is the threshold between laminar and turbulent flow inside a tube [8]. Measurements of air flow rate and pressure drop in the tube (not shown) also indicate that the flow transitions from laminar to turbulent at 3500 mL/min. We conclude that transport efficiency increases with increasing flow rate in the laminar regime but decreases in the turbulent regime, probably due to air vorticities inside the tube.

Figure 4(b) shows that the transport efficiency increased when the tube inlet was positioned closer to the sample. This increase in efficiency can be attributed to an increase in air velocity around the heated tip rather than the air flow rate through the tube. The plume of desorbed molecules may be much smaller than the tube due to the large difference between the depth of desorbed region (~ 4 µm) and the tube ID (2.1 mm) [10].This indicates that the most of the air flow would not interact with the plume, and thus the transport will not be governed by the mass flow rate into the tube but the air velocity around the plume. The transport efficiency as a function of the tip-tube inlet distance decreases similarly to the calculated air velocity along the tube (solid red line). This similarity suggests that

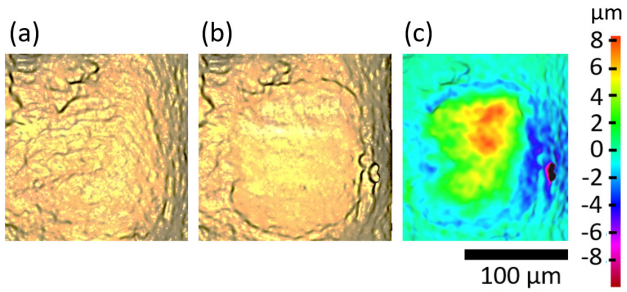

Figure 2: Three-dimensional optical microscopy measurements of the sample (a) before and (b) after thermal desorption. (c) False-color image of the difference in height between each image. A positive value represents the desorbed area, and the negative value represents partial re-deposition.

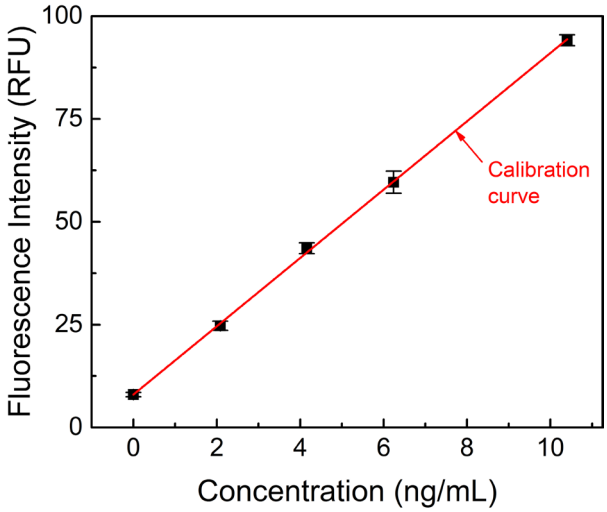

Figure 3: Fluorescence plate reader calibration curve plotted over 9AA concentrations from 0 – 10 ng/mL. Excitation wavelength and emission wavelength were set at 400 nm and 470 nm respectively to maximize the signal to noise ratio of 9AA in ethanol solution. Each concentration was measured with 10 technical replicates.

the transport efficiency is governed by air velocity around the sample rather than the total mass flow rate through the tube as reported in the literature [4].

Figure 4(c) shows that for a given mass flow rate, transport efficiency increases as the tube diameter decreases. The smaller diameter tube results in higher air velocity, which in turn drives higher inhalation efficiency and lower residence time in the tube.

Figure 5(a) shows the transport efficiency at different tube temperatures. Heating the tube is a commonly used method to reduce the analyte adsorption to the tube interior [3-5]. However, the transport efficiency decreased when the tube was heated above 100 ˚C. We attribute this decrease in efficiency to an increase in temperature of the well plate from the impinging hot air, decreasing the quantity of captured material. Thus, although the tube heating might help to reduce the sample adsorption within the tube, it seems to worsen the transport efficiency in decoupled AFM-MS systems.

Figure 5(b) shows the analyte adsorption to the tube

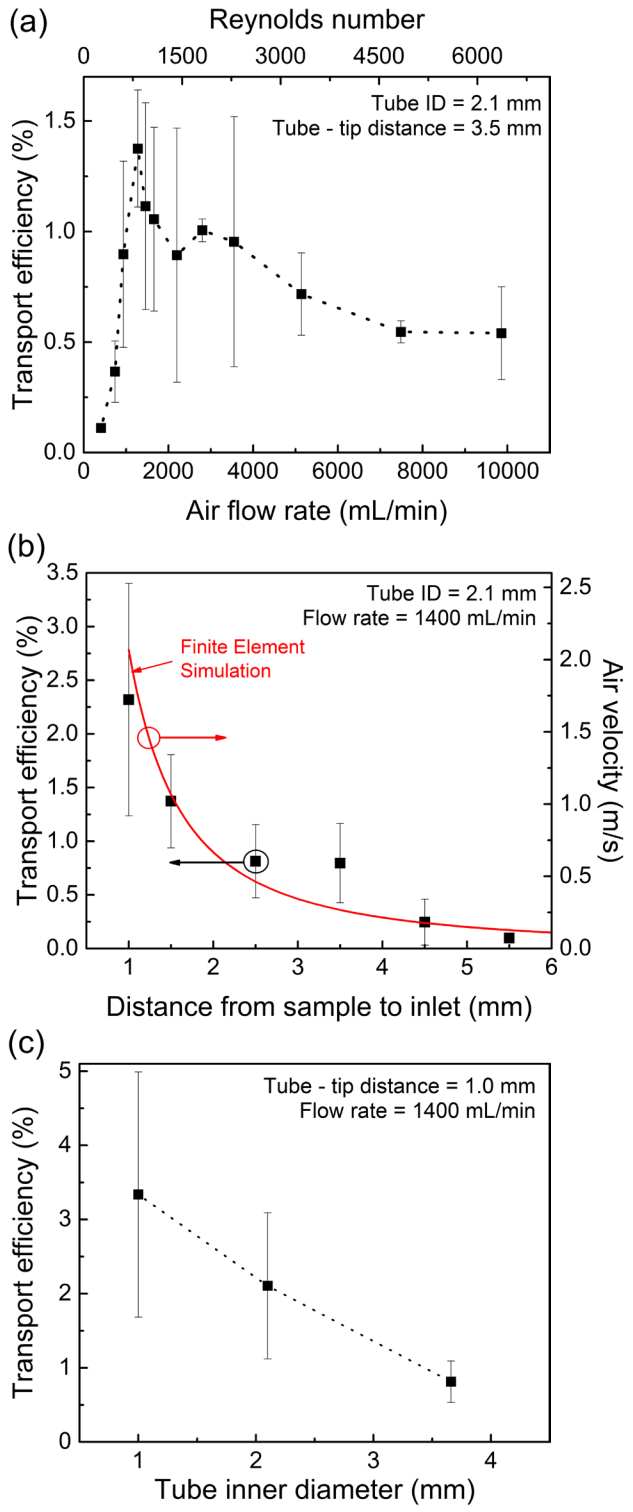

Figure 4: Effect of tube parameters on the transport efficiency. (a) Dependence on air flow rates. (b) Dependence on distance from sample to the tube inlet. The solid red line shows a finite element analysis prediction. (c) Dependence on tube inner diameters at a constant air flow rate of 1400 mL/min.

interior at different axial positions of the tube, which is defined as the adsorbed mass at each position to the total desorbed mass. To measure the adsorbed analyte distribution, we cut the 21 cm-long tube into 20 pieces after a thermal desorption process at the flow rate of 1400 mL/min. Each piece was separately washed in ethanol solvent, and the adsorbed mass was calculated from the fluorescence intensity and the calibration curve. Without tube heating, the total analyte adsorption was about 10%. More than half of the adsorption occurred in the front 5 cm of the tube, and the rest of the tube had relatively small adsorption at ~ 0.25% per cm. We also observed that the tube outlet region had a larger adsorption than the middle. This may have been induced by air vortices near the exit. Tube heating successfully reduced the analyte adsorption to tube interior, as shown in Figure 5(b).

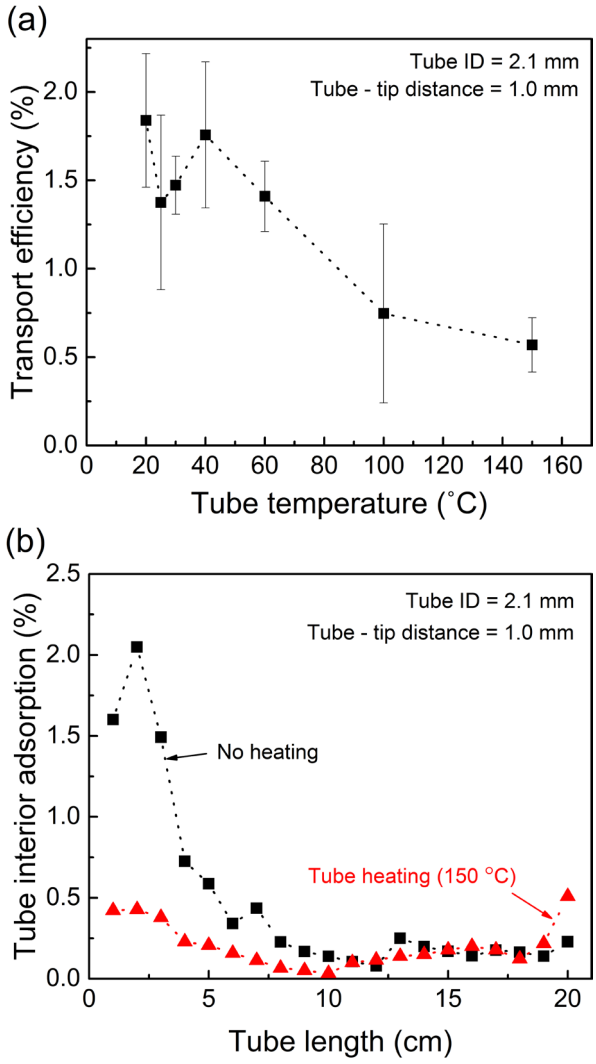

Figure 5: Effect of tube heating on sampling. (a) Transport efficiency at different tube temperatures. Transport efficiency decreases when the tube temperature is higher than 60 ˚C, which is attributed to heating of the collecting region of the well plate. (b) The sample adsorption on the tube inner wall. When the tube is heated to 150 ˚C, the adsorption on the tube inner wall decreases significantly.

In order to find the highest signal to noise with our system, we conducted the entire process of AFM-MS with 9AA under optimal transport conditions as identified above. The tip-tube distance was 1 mm, the tube diameter was 1.0 mm, the tube length was 20 cm, the flow rate was 1400 mL/min, and the tube temperature was 25 ˚C. For

these experiments, the analyte was collected on a polished aluminum substrate. The collected 9AA was detected and analyzed with laser desorption/ionization mass spectrometry on a Bruker ultrafleXtreme. A 365 nm laser irradiated the analyte with a frequency of 2000 Hz. The mass spectra were obtained from 500 summed laser pulses. Positive ions with *m/z* of 100—500 were collected. Figure 6 shows mass spectra acquired from a region where 9AA was deposited on the aluminum substrate. The base peak at *m/z* 195.1 corresponds to the protonated molecular ion for 9AA. The mass spectra obtained from the blank region shows negligible noise and no perceivable *m/z* 195.1 peak. The mass spectra intensity of noise is less than 100 in arbitrary unit, thus the signal to noise ratio is about 50.

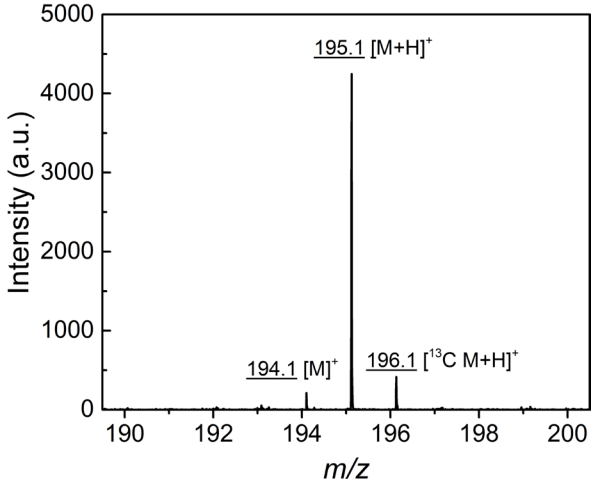

Figure 6. Mass spectra obtained from laser desorption/ioinization of the collected 9AA sample on an aluminum MALDI target.

CONCLUSIONS

This paper reports transport physics of the sampling process in an AFM-MS system. The transport efficiency of the system was measured by comparing the thermally desorbed mass to collected mass. The effects of tube parameters including air flow rate, distance from the sample to tube inlet, and tube inner diameter on the transport efficiency were measured and discussed. The transport efficiency became optimal under the following conditions: (1) highest air flow in laminar regime, (2) smallest distance from sample to tube inlet, and (3) smallest tube inner diameter. The effect of tube length was also studied by measuring the tube interior adsorption. Tube length was not a significant parameter unless it is shorter than 5 cm. Lastly, transport efficiency was measured at different tube temperatures, which suggests that the higher temperature may worsen the overall collection efficiency in decoupled AFM-MS systems.

ACKNOWLEDGEMENTS

We thank Dr. Craig Prater at Anasys Instruments for valuable discussions. JVS acknowledges support through NSF CHE 16-067915.

REFERENCES

[1] T. J. Comi et al., "Categorizing Cells on the Basis of their Chemical Profiles: Progress in Single-Cell Mass Spectrometry", J. Am. Chem. Soc., vol. 139, pp. 3920-3929, 2017.

[2] R. Zenobi et al., "Single-Cell Metabolomics: Analytical and Biological Perspectives", Science, vol. 342, 2013.

[3] O. Ovchinnikova *et al.*, "Combined atomic force microscope based topographical imaging and nanometer-scale resolved proximal probe thermal desorption/ electrospray ionization-mass spectrometry", *ACS Nano.*, vol. 5, pp. 5526-5531, 2011.

[4] O. Ovchinnikova *et al.*, "Atomic force microscope controlled topographical imaging and proximal probe thermal desorption/Ionization mass spectrometry imaging", *Anal. Chem.*, vol. 86, pp 1083-1090, 2013.

[5] O. Ovchinnikova *et al.*, "Co-registered Topographical, Band Excitation Nanomechanical, and Mass Spectral Imaging Using a Combined Atomic Force Microscopy/Mass Spectrometry Platform", *ACS Nano.*, vol. 9, pp. 4260–4269, 2015.

[6] S. Ghorai *et al.*, "Tip-Enhanced Laser Ablation Sample Transfer for Biomolecule Mass Spectrometry", *J. Am. Soc. Mass Spectrom.*, vol. 26, pp. 63–70, 2015

[7] J. Lee *et al.*, "Electrical, thermal, and mechanical characterization of silicon microcantilever heaters", *J. Microelectromech. Syst.*, vol. 15, pp. 1644-1655, 2006.

[8] W. Kays et al., *Convective Heat and Mass Transfer*, McGraw-Hill Companies, Inc., Ohio, 2012

[9] L. Zhu et al., "Atmospheric Pressure Sampling for Laser Ablation Based Nanoscale Imaging Mass Spectrometry: Ions or Neutrals?", *J. Phys. Chem. C,* vol. 115, pp. 1006-1013, 2011

[10] T. A. Schmitz et al., "Characterization of aerosol plumes in nanosecond laser ablation of molecular solids at atmospheric pressure", *Appl. Phys. B*, vol. 100, pp. 521-533, 2010

CONTACT

*W.P. King, wpk@illinois.edu